COMPDYN 2025
10th ECCOMAS Thematic Conference on
Computational Methods in Structural Dynamics and Earthquake Engineering
M. Papadrakakis, M. Fragiadakis (eds.)
Rhodes Island, Greece, 15-18 June 2025

RISK-TARGETED GROUND MOTIONS: INSIGHTS FROM A CASE-STUDY APPLICATION ON ITALIAN SITES

Georgios Baltzopoulos[1], Antonio Grella[1], and Iunio Iervolino[1,2]

[1] Dip. di Strutture per l'Ingegneria e l'Architettura, Università degli Studi di Napoli Federico II
Via Claudio, 21, 80125, Napoli, Italy
georgios.baltzopoulos@unina.it

[2] IUSS – Scuola Universitaria Superiore di Pavia
Piazza della Vittoria 15, 27100, Pavia, Italy
{antonio.grella, iunio.iervolino}@unina.it

Abstract

Research on performance-based earthquake engineering has shown that designing building structures using seismic actions chosen based on the same return period of exceedance at different sites, does not necessarily warrant the same reliability. This has prompted several proposals for alternative seismic design actions, referred to as risk-targeted, aimed at ensuring consistent failure risk across sites with varying levels of earthquake hazard. This study adapts the provisions of the US National Earthquake Hazard Reduction Program (NEHRP) for the design of regular moment-resisting reinforced concrete buildings across multiple Italian sites. For each location, a risk-targeted design response spectrum is defined by selecting a desired failure risk threshold that aligns with the requirements of Eurocode 8. The sites were specifically selected to represent sufficiently high hazard levels so that the lateral strength demand for the case-study buildings should be at least apparently governed by seismic base shear, rather than other design considerations. The failure risk for these buildings was evaluated using incremental dynamic analysis (IDA) of simplified numerical models to determine fragility, which was subsequently integrated with site-specific hazard curves. The IDA utilized different ground shaking intensity measures, each with distinct sufficiency and efficiency characteristics. The findings reveal a potential discrepancy between the initially set risk target and the post-analysis calculated risk, which is partly attributed to known limitations of spectral ordinates as intensity measures to express fragility when failure is related to collapse, and the design procedure's sensitivity to some assumptions. Additionally, at low-hazard sites, the risk-targeted spectra appear to be interchangeable with traditional uniform hazard spectra, while at high-hazard sites there is a more notable difference between the two.

Keywords: Risk-targeted design, seismic hazard, structural reliability.

1 INTRODUCTION

Most modern building codes espouse the principles of performance-based earthquake engineering, requiring the design verification for performance objectives to be made against seismic actions whose rarity depends on the importance of the structure and objective. In this context, some building codes [1,2] define the seismic actions according to a uniform-hazard approach, which entails that the design ground motion maintains the same return period of exceedance, T_r, across different sites. However, recent studies have shown that the seismic structural reliability, expressed in terms of annual failure rate, λ_f, tends to be lower in areas with higher earthquake hazard than at those with low hazard [3], even though, under uniform-hazard approach, the elastic lateral strength demand varies commensurate with site-specific hazard analysis [4]. This could be possibly attributed to differences in hazard curve shape from one site to another, especially at shaking intensities whose return periods go beyond the ones typically considered for design [5] and to the lack of explicit control over seismic overstrength of structures during the design process [6,7].

One of the proposals that have emerged to alleviate this discrepancy in seismic reliability among sites, is to move away from uniform-hazard design ground motions towards so-called risk-targeted ground motions (RTGMs). RTGMs are design actions that are defined with the explicit goal of achieving a desirable level of seismic reliability, quantified by means of a target failure rate, λ_f^* [8], that is an annual rate of failing to meet a seismic performance objective. This approach typically entails making some a-priori assumptions about the corresponding structural fragility, which is defined as the conditional probability of failure, given the value of shaking intensity [9,10]. For example, this approach currently underlies the definition of design ground motions in north American standards [11].

Although the RTGM approach has been recently gaining traction with the earthquake engineering community [12,13], its implementation has been documented to still present some challenges [14]. For example, the authors have observed that various factors that enter into practical design applications tend to limit the risk homogenization potential of RTGMs [15]. This work builds upon those past observations to further explore the application of RTGMs at six Italian sites, for three different performance objectives, that is varying target reliabilities associated with a condition of conventional *global collapse*. More specifically, a mid-rise reinforced concrete (RC) moment-resisting frame is considered as benchmark structure, whose design against RTGM seismic actions is simulated across all sites considered. These alternative designs are simulated using available results of a recent extensive research project [16]. Subsequently, their seismic reliability is calculated using incremental dynamic analysis (IDA; [17]) on equivalent inelastic single degree-of-freedom (SDoF) systems to procure their collapse fragility curves, which are then integrated with seismic hazard. Finally, these RTGMs are compared to nominally equivalent uniform-hazard design ground motions.

2 RISK-TARGETED DESIGN SPECTRA AND SIMULATED DESIGN

The definition of a RTGM, generally requires the definition of a reliability objective and of a value of *failure* probability, given the design shaking intensity. In this context, failure is defined as the loss of structural performance beyond a predetermined threshold. Here the collapse limit state is considered; this is to be interpreted as dynamic instability of the structure, whose numerical prediction is sometimes termed the IDA flatline point [18]. For the present study, three alternative reliability objectives are considered, in terms of target annual failure rate, λ_f^*; specifically, the values of $\lambda_f^* = \{2 \cdot 10^{-4}; 1 \cdot 10^{-4}; 6 \cdot 10^{-5}\}$ are considered. Finally, the adopted anchoring value for the conditional failure probability is $P[f|Sa(T) = sa_{RT}] = 0.10$, where $Sa(T)$ denotes the spectral pseudo-acceleration at vibration period T, sa_{RT} is the RTGM intensity and f represents structural failure, as defined above. Note that this conditional failure probability is also termed the collapse fragility of the structure.

Herein, risk-targeted design spectra are generated for six Italian sites. They were selected to cover a representative range spanning conditions from *high*- to *low*-hazard in relative terms. The RTGM generation assumes that the seismic fragility, defined by the probability distribution of shaking intensity $Sa(T)$ leading to structural failure, follows a lognormal model with an assigned standard deviation $\beta = 0.6$. Consequently, the value of sa_{RT} can be determined according to the iterative procedure shown in the flowchart of Figure 1.

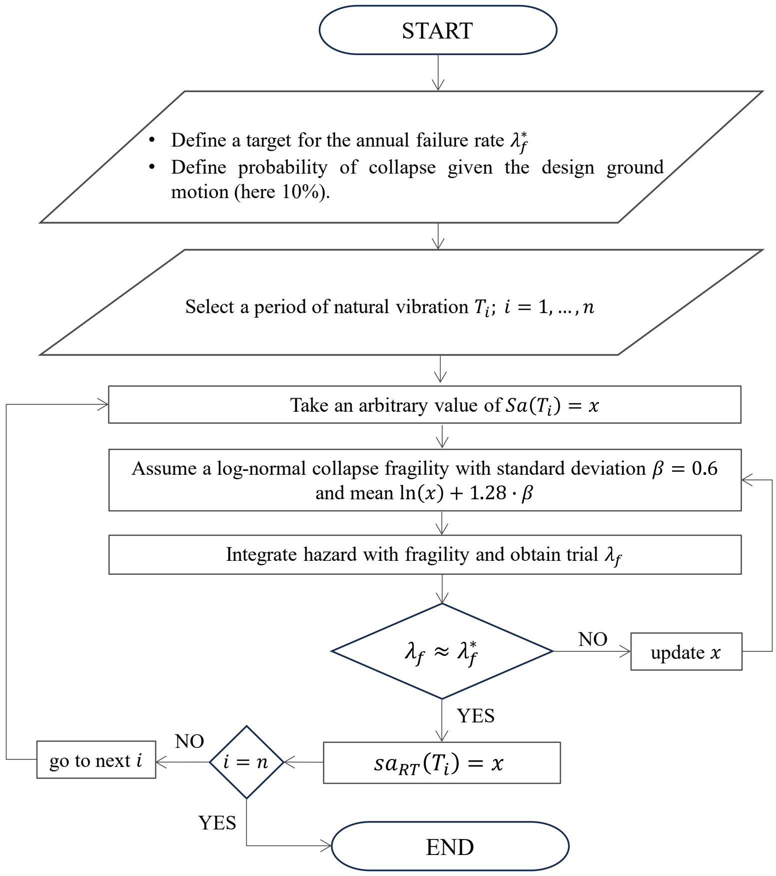

Figure 1. Flow-chart of the RGTM definition procedure.

As shown in the chart, for each site, target λ_f^* and vibration period, a series of iterations are performed. First, an arbitrary spectral acceleration value is assigned to sa_{RT} and the annual failure rate at the site, λ_f, is calculated as:

$$\lambda_f = \int_0^{+\infty} \Phi\left[\frac{\ln(Sa) - \ln(sa_{RT}) - 1.28 \cdot \beta}{\beta}\right] \cdot |d\lambda_{Sa}|, \tag{1}$$

where $\Phi(\cdot)$ denotes the standard Gaussian function, and λ_{Sa} is the annual rate of earthquakes exceeding each $Sa(T)$ value at the construction site, that is, the hazard curve. This process is iterated by updating the sa_{RT} value, until λ_f approaches the target value λ_f^*, and is then repeated for all vibration periods and all the sites. In this equation, the expression $\ln(sa_{RT}) + 1.28 \cdot \beta$ corresponds to the median spectral acceleration causing failure, consistent with the assumption that sa_{RT} corresponds to the 10-th percentile of the collapse fragility.

Prior to this calculation, a probabilistic seismic hazard analysis (PSHA; [19]) was conducted to determine λ_{Sa} for each site. The REASSESS software [20] for PSHA was employed, for a range of vibration periods spanning $0s \leq T \leq 2s$, using the ground motion prediction model suggested by Ambraseys and co-authors [21]. The analysis was based on the seismic source model for Italy [22], which is also adopted in the current building code. These calculations were performed for site class type C, according to Eurocode 8 classification [2].

The computed risk-targeted spectra are shown in Figure 2, for all six sites examined and for the three target failure rates. The failure probability over a 50-year period, $P_{f,50y} = 1 - e^{-\lambda_f^* \cdot 50}$, corresponding to each target annual failure rate, is reported in Table 1. These sites are grouped into high- to medium-hazard sites (Udine, Cortino, L'Aquila and Brienza) and low-hazard sites (Napoli and Arezzo). From panel A to C is observed that the seismic actions from RTGM tend to increase as the performance objective becomes more stringent (i.e., lower annual failure rates), which corresponds to higher seismic actions required to ensure lower failure probability.

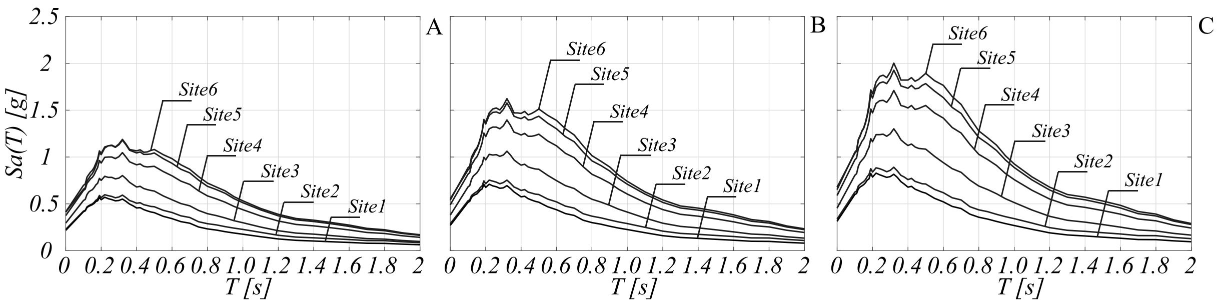

Figure 2. Risk-targeted spectra for the six case-study sites, considering a target annual failure rate of $\lambda_f^* = 2 \cdot 10^{-4}$ (A), $\lambda_f^* = 1 \cdot 10^{-4}$ (B), and $\lambda_f^* = 6 \cdot 10^{-5}$ (C).

λ_f^*	$2 \cdot 10^{-4}$	$1 \cdot 10^{-4}$	$6 \cdot 10^{-5}$
$P_{f,50y}$	1%	0.5%	0.3%

Table 1. Target annual rates and corresponding collapse probabilities in 50 years.

Furthermore, additional PSHA calculations were performed to obtain hazard curves for a more advanced intensity measure (IM), that is average spectral acceleration Sa_{avg}, which is defined as the geometric mean of 5% damped spectral accelerations at vibration periods $T_i, i = 1,2,\ldots,N$:

$$Sa_{avg} = \left[\prod_{i=1}^{N} Sa(T_i)\right]^{\frac{1}{N}}, \tag{2}$$

where $N = 17$ is the number of spectral ordinates contemplated in the aforementioned ground motion model with $T \geq 0.7s$. This choice is motivated by the fact that this specific IM has a larger predictive power of inelastic displacement response compared to $Sa(T)$, attributed to its consideration of the spectral shape beyond the structure's fundamental period [23], which enhances the failure probability assessment [24–26]. To compute these hazard curves, the same ground motion as before was used, along with a cross-correlation model among spectral ordinates [27]. The locations of the sites, and their $\lambda_{Sa_{avg}}$ hazard curves, are shown in Figure 3.

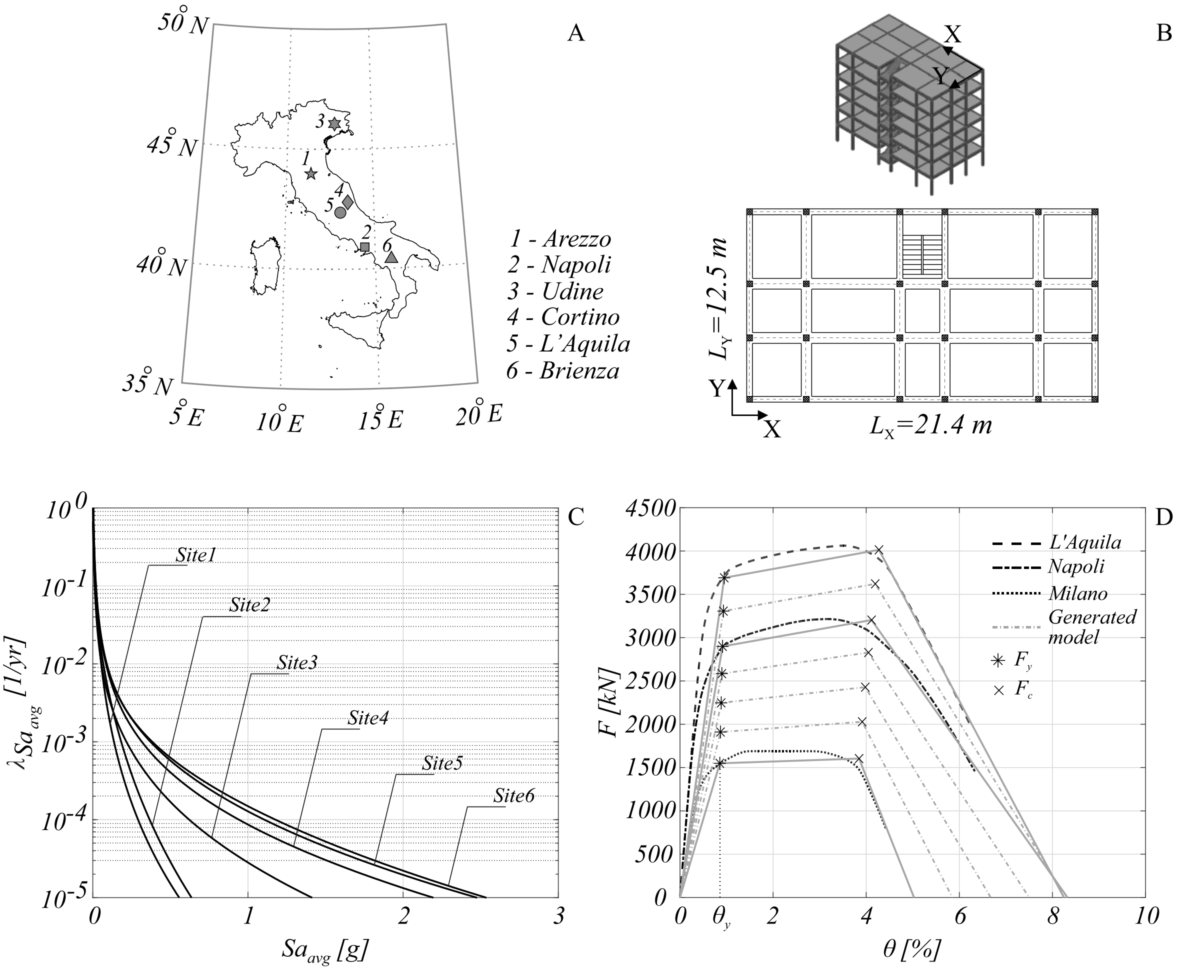

Figure 3. Map of Italy showing the six case-study sites (A); elevation and plan of the six-storey buildings (B); average spectral acceleration hazard curves (C); reference static pushovers of the six-storey reinforced concrete buildings and generated backbones at intermediate base shears (D).

For the present study, a six-storey RC bare frame building is considered and its design against the RTGM obtained for each site is simulated. The elastic base shear demand per main structure's direction, F_e, is assumed to only reflect the contribution of the corresponding fundamental period of vibration T_1, as is common for moment-resisting mid-rise frames, calculated as:

$$F_e = m^* \cdot \Gamma \cdot \left[\frac{Sa_e(T_1)}{q}\right], \tag{3}$$

where $Sa_e(T_1) = (2/3) \cdot sa_{RT}$ is the elastic spectral acceleration demand, with a two-thirds reduction of the RTGM according to the procedure outlined in FEMA 695 [28], m^* is the equivalent mass of the corresponding SDoF oscillator, Γ is the modal participation factor and q is the maximum allowable code-mandated *behavior factor*. The latter links the elastic demand to the local ductility demands in members and hence to the plastic deformation of the structure under the design ground motion, with a value of $q = 3.9$ considered for the specific frame type.

The result of simulated design at each site are two surrogates inelastic SDoF structures, one per principal direction of the structure, identified by the acronyms 6st-X and 6st-Y. These SDoF systems exhibit a trilinear backbone, that is a monotonic force-displacement response curve [29], having a peak strength of $F_c = \alpha_u \cdot F_e$, with α_u being the overstrength coefficient. In a previous work [30], the authors used the static pushover (SPO) results [16] of alternative designs of this six-storey frame, each designed according to the Italian building code at sites with different seismicity, to generate families of equivalent SDoF systems with different lateral strength. The X-direction SPO curves from the three original designs at L'Aquila, Napoli and Milano (in decreasing order of seismic hazard) are shown in Figure 3.D. These curves are expressed in terms of base shear, F, and roof drift, θ, and are shown alongside their trilinear approximations, as well as interpolations generated for intermediate strength values.

For the purposes of the simulated design, the parameters m^*, Γ, T_1, α_u for both directions are obtained via iterative interpolation between the original reference structural design data, leading to assigning a surrogate trilinear-backbone SDoF consistent with the elastic base-shear demand stemming from Equation (3). It should be noted that the vibration period of the equivalent inelastic SDoF oscillator, T^*, is generally different from T_1 , which is the period obtained from the design elastic model of the structure. This difference is because the latter is the result of an approximation of the secant stiffness at yield, via a nominal 50% reduction of member sections' moments of inertia, while the former is calculated as:

$$T^* = 2\pi \cdot \sqrt{m^* \cdot \delta_y^* / F_y^*}, \tag{4}$$

where F_y^* is the nominal yielding force, $\delta_y^* = H \cdot \theta_y / \Gamma$ is the displacement corresponding to the development of a plastic mechanism, $\theta_y \approx 0.8\%$ is the corresponding roof drift [31,32], and H is the building height.

3 COMPARING SEISMIC RELIABILITY AMONG SITES

To calculate the seismic reliability resulting from these simulated designs, expressed in terms of λ_f, structural fragility was analytically evaluated based on IDA of the SDoF oscillators, using the forty-four accelerograms of the FEMA-P695 far-field set [28]. The analyses were conducted using the DYANAS [33] interface for OpenSees [34] and two sets of IDA curves were obtained for each case: one by scaling the records first to common $Sa(T_1)$ levels and another by subsequently scaling to a common Sa_{avg}. From each analysis, the flat-line height of the IDA curves was used to identify the IM level causing failure, and lognormal fragility curves were fitted to the results [35], expressed in terms of both $Sa(T_1)$ and Sa_{avg}. The annual failure rates, corresponding to the three alternative levels of target seismic reliability considered, were derived by integrating the fragility functions with the respective hazard curves at each site:

$$\lambda_f = \int_0^{+\infty} P[f|IM = im] \cdot |d\lambda_{im}|, \tag{5}$$

where $P[f|IM = im]$ is the IDA-based fragility lognormal fragility function and IM represents either $Sa(T_1)$ or Sa_{avg}.

The results of this operation are summarized in Figure 4, where non-filled markers are used to indicate the annual failure rates of structures whose intrinsic base-shear capacity, stemming from detailing due to gravity-load design and minimum code requirements, overrides the risk-targeted seismic demand. On the other hand, filled markers are used to indicate cases where RTGM seismic demand governs lateral resistance. The first observation is that, in all cases, the analytical reliability estimates appear to have overshot the target performance objectives λ_f^*, especially considering the Sa_{avg} based calculations, which is the main point of reference. This can be attributed to overstrength, which is partly due to $Sa_e(T_1) > Sa_e(T^*)$.

The second observation that can be made is regarding the dispersion of the failure rates. For this consideration and for each performance objective, the failure rates' arithmetic means, $\bar{\lambda}$, and standard deviations, s, are calculated only for those designs that are governed by the seismic actions, that is for the points on the plot with shaded markers; the location of the means are indicated on the graph by a dash-double-dot line, while the actual values are reported in Table 2. The table also reports their empirical coefficient of variation, $CoV = s/\overline{\lambda}$.

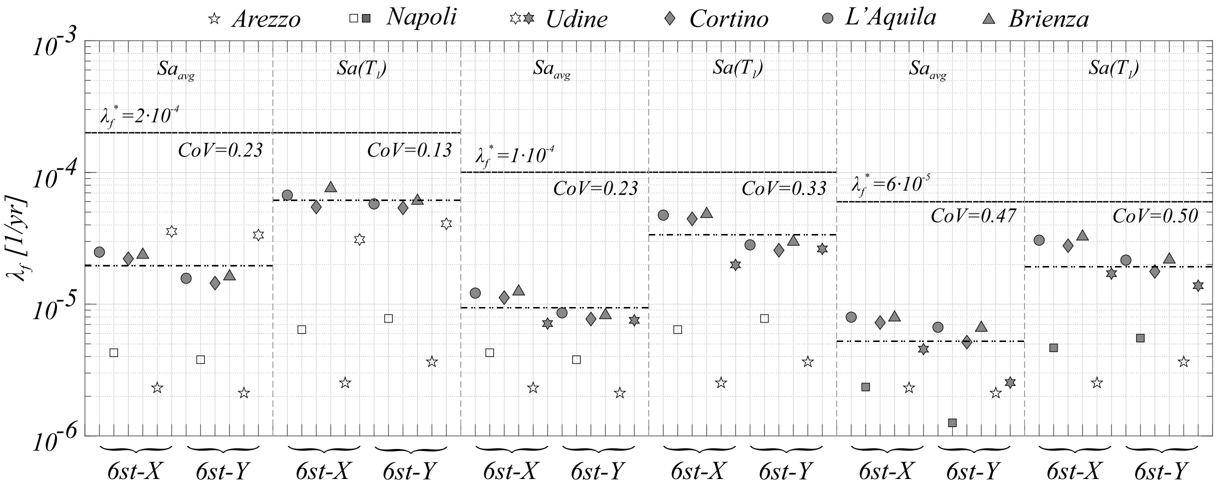

Figure 4. Annual failure rates for the two structural configurations at six sites, using two alternative intensity measures, as interfacing variables between fragility and hazard, and three target annual failure rates.

Performance objective	Sa_{avg}			$Sa(T_1)$		
	$\overline{\lambda}$	s	$s/\overline{\lambda}$	$\overline{\lambda}$	s	$s/\overline{\lambda}$
	$1 \cdot 10^{-5}$ [1/yr]			$1 \cdot 10^{-5}$ [1/yr]		
$\lambda_f^* = 2 \cdot 10^{-4}$	1.950	0.455	0.23	6.164	0.846	0.13
$\lambda_f^* = 1 \cdot 10^{-4}$	0.938	0.219	0.23	3.373	1.117	0.33
$\lambda_f^* = 6 \cdot 10^{-5}$	0.523	0.246	0.47	1.931	0.959	0.50

Table 2. Values of the mean and standard deviation of the annual failure rates, estimated varying the intensity measure for deriving the fragility functions and the performance objectives.

Although it seems that the empirical standard deviation of the failure rates is smaller when using Sa_{avg} as the interfacing variable between hazard and fragility, rather than $Sa(T_1)$, this can be partly attributed to the mean estimates obtained using the former IM, being smaller than those derived using the latter. In fact, if one considers the CoV, which expresses the standard deviation using the mean as the unit of measure, this trend for dispersion is not univocal. It is also important to note that these results are subject to estimation uncertainty [36], as the failure rates are derived from finite samples of structural response, and the two IMs are not characterized by the same *efficiency* [37].

A more interesting trend is the fact that the CoV of the failure rates either stays the same or increases, when moving from one performance objective to a more stringent one, that is moving towards situations where the same structure has to be designed with greater lateral resistance, due to higher RTGMs. Also in this case, it is preferable to monitor the dispersion of reliability estimates by following the CoV, since $\overline{\lambda}$ will naturally decrease when moving to lower λ_f^* targets. This trend can be explained by the fact that, as the reliability target drops to lower failure rates, low-hazard sites pass from a condition where reliability is not governed by seismic design, to one where the more stringent performance objective makes seismic design relevant. This can be visualized in the graph, by noticing empty site-specific markers that become filled going from left to right, that is from $\lambda_f^* = 2 \cdot 10^{-4}$ towards $\lambda_f^* = 6 \cdot 10^{-5}$. It is those sites that exhibit the largest deviations from the mean reliability in the last third of the graph. In other words, lowering the target reliability towards more demanding performance objectives, appears to tend to reduce the risk harmonization potential of RGTMs, as these seismic design actions tend to become relevant for lower-hazard sites.

4 RISK-TARGETED VS UNIFORM-HAZARD SPECTRA

By construction, the RTGM spectral ordinates depend on some assumptions about structural fragility, a target reliability objective and the site-specific seismic hazard. Therefore, the sa_{RT} values, at different vibration periods, will not necessarily have the same return period, T_r. Nevertheless, after the $sa_{RT}(T)$ have been defined, it is straightforward to look at the hazard curves used to derive them and calculate $T_r = 1/\lambda_{sa_{RT}}$ for each T. The results of this operation, for all sites and performance objectives considered here, are shown in Figure 5.A.

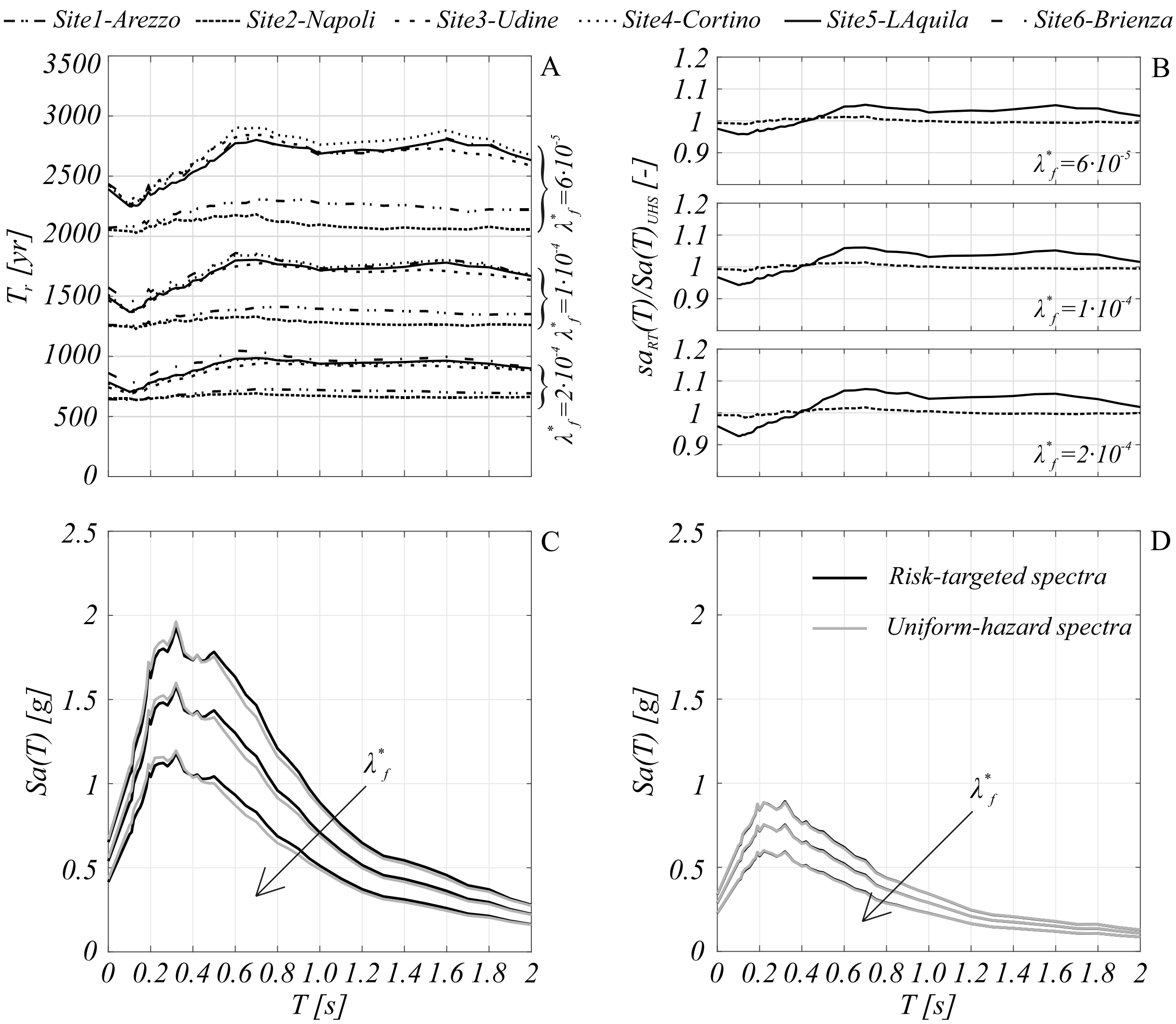

Figure 5. Comparison between the design spectra. Return period and vibration periods relationship (A); ratio between the risk-targeted spectral acceleration and uniform hazard spectral acceleration (B); risk-targeted spectra for the case-study sites of L'Aquila (C) and Napoli (D) along with the comparison uniform-hazard spectra.

From the figure, one can observe that for the high-seismic hazard sites, the variability of T_r among the RTGM spectral ordinates is more marked than for low-seismic hazard sites; this is especially evident for Sites 1 and 2 at the two lower performance objectives, for which the T_r

appears almost constant across the 0 to 2s vibration period range shown. To better illustrate this trend, a comparison uniform-hazard spectrum, $Sa(T)_{UHS}$, was defined for each performance objective, at Site 2 (Napoli) and Site 5 (L'Aquila). These comparison UHS were defined for each case, by taking the average-across-vibration-periods T_r of the RTGM (within the 0s to 2s interval), which are reported case-by-case in Table 3, and then obtaining the spectral ordinates corresponding to that mean T_r from the hazard curves.

Site	$\lambda_f^* = 2 \cdot 10^{-4}$	$\lambda_f^* = 1 \cdot 10^{-4}$	$\lambda_f^* = 6 \cdot 10^{-5}$
Site2-Napoli	665 years	1280 years	2100 years
Site5-L'Aquila	870 years	1620 years	2550 years

Table 3. Mean return periods of the RTGMs, used to construct uniform hazard spectra for comparison.

Figure 5.B plots the ratio $sa_{RT}(T)/Sa(T)_{UHS}$ against T, for the two sites, and three performance objectives, while the actual RTGM and UHS spectra under comparison are shown in the panels below. For the lower-hazard site of Napoli, this ratio remains within the range of 0.99 and 1.02, that is close to unity. On the other hand, for the higher-hazard site of L'Aquila, the ratio exhibits more variation, but the two ordinates never differ by more than 10% in this period range. In fact, it appears that the uniform-hazard ordinates are higher than the risk-targeted ones for $T < 0.4s$ and vice-versa for $0.4s < T < 2.0s$, but this could depend on the ground motion prediction model used in these specific hazard calculations and bears investigating further. This comparison seems to suggest that, for low-seismic-hazard sites, RTGM and UHS whose return period has been explicitly calibrated against the declared performance objective, can be almost interchangeable. It should also be noted that, in this comparison, neither the risk-targeted nor the uniform-hazard spectra were modified to comply with a more code-friendly standardized design spectrum shape, which is another issue [14]. This is highlighted because the percentile differences observed between the compared spectra appear similar to those that one could plausibly expect when fitting calculated spectral ordinates to a code-standard design spectrum shape.

5 DISCUSSION AND CONCLUSIONS

The presented study examined an application of risk-targeted ground motions to the design of a single case-study reinforced concrete frame structure, which was repeated for multiple Italian sites characterized by varying seismic hazard. The applications considered three alternative performance objectives, in terms of the target annual collapse rate. The analysis confirmed that the ability of RTGM-based seismic actions to harmonize structural reliability, for the same structural typology designed across sites with different seismic hazard levels, can be limited for several reasons. One reason can be found in the simplifying assumptions inherent in designing against elastic demand, with performance objectives that would have the structure into the plastic deformation range. Another reason is the non-optimal performance of first-mode spectral acceleration as an intensity measure to predict global collapse. Both of these observations confirm previous works on the topic.

One interesting observation that emerged from this study concerns the role of low-hazard sites when evaluating the ability of RTGMs to harmonize seismic risk between different construction locations. In construction sites affected by lower levels of seismic hazard, it often occurs that the ability of the structure to resist earthquake-induced lateral forces is determined by code-mandated minimum detailing requirements or design against other types of actions, rather than the seismic design actions themselves. Thus, it is reasonable to disregard those sites when evaluating the level of risk uniformity achievable by RTGMs. Nevertheless, in cases where performance objectives need to become more stringent, for example because of strategic importance of a structure and/or longer required service life, RTGM-based actions can return to govern lateral resistance, and those low-hazard sites re-emerge as the problem child that limits the risk harmonization potential of RTGMs.

A second observation regards the innate difference in form between a set of uniform-hazard and risk-targeted spectral ordinates, that is the difference in spectral shape prior to any modifications to fit a canonical code-mandated form. For the case-study applications considered herein and all the underlying models and assumptions, it was shown that, for the low-hazard sites, it is possible to define uniform-hazard spectra that are almost undistinguishable from their risk-targeted counterparts. For the higher-hazard sites such an operation was not possible, but even then, the period-dependent deviation of the risk-targeted from the uniform-hazard spectrum was mostly within 5% and never exceeded 10%.

REFERENCES

1. CS.LL.PP. Norme Tecniche per Le Costruzioni. *Gazzetta Ufficiale della Repubblica Italiana* **2018**, *42*.
2. CEN *EN 1998-1: Eurocode 8 - Design of Structures for Earthquake Resistance. Part 1: General Rules, Seismic Actions and Rules for Buildings*; European Committee for Standardization, 2004; ISBN 5947185067.
3. Iervolino, I.; Spillatura, A.; Bazzurro, P. Seismic Reliability of Code-Conforming Italian Buildings. *Journal of Earthquake Engineering* **2018**, *22*, 5–27, doi:10.1080/13632469.2018.1540372.
4. McGuire, R.K. Probabilistic Seismic Hazard Analysis and Design Earthquakes: Closing the Loop. *Bulletin - Seismological Society of America* **1995**, *85*, 1275–1284, doi:10.1016/0148-9062(96)83355-9.
5. Iervolino, I.; Giorgio, M.; Cito, P. The Peak over the Design Threshold in Strong Earthquakes. *Bulletin of Earthquake Engineering* **2019**, *17*, 1145–1161, doi:10.1007/s10518-018-0503-9.
6. Žižmond, J.; Dolšek, M. Evaluation of Factors Influencing the Earthquake-Resistant Design of Reinforced Concrete Frames According to Eurocode 8. *Structure and Infrastructure Engineering* **2016**, *12*, 1323–1341, doi:10.1080/15732479.2015.1117112.
7. Ricci, P.; Di Domenico, M.; Verderame, G.M. Behaviour Factor and Seismic Safety of Reinforced Concrete Structures Designed According to Eurocodes. *Structures* **2023**, *55*, 677–689, doi:10.1016/j.istruc.2023.06.060.
8. Luco, N.; Ellingwood, Bruce R. Hamburger, Ronald O. Hooper, J.D.; Kimball, J.K.; Kircher, C.A. Risk-Targeted versus Current Seismic Design Maps for the Conterminous United States 2007.
9. Douglas, J.; Ulrich, T.; Negulescu, C. Risk-Targeted Seismic Design Maps for Mainland France. *Natural Hazards* **2013**, *65*, 1999–2013, doi:10.1007/s11069-012-0460-6.
10. Silva, V.; Crowley, H.; Bazzurro, P. Exploring Risk-Targeted Hazard Maps for Europe. *Earthquake Spectra* **2016**, *32*, 1165–1186, doi:10.1193/112514EQS198M.
11. ASCE *ASCE/SEI 7-22 Minimum Design Loads and Associated Criteria for Buildings and Other Structures*; American Society of Civil Engineers, 2022; ISBN 9780784415787.
12. Iervolino, I. Risk-Targeted Seismic Design: Prospects, Applications, and Open Issues, for the next Generation of Building Codes. *Earthq Eng Struct Dyn* **2023**, *52*, 3919–3921, doi:https://doi.org/10.1002/eqe.3999.

13. Žižmond, J.; Dolšek, M. Formulation of Risk-targeted Seismic Action for the Force-based Seismic Design of Structures. *Earthq Eng Struct Dyn* **2019**, *48*, 1406–1428, doi:10.1002/eqe.3206.
14. Spillatura, A.; Vamvatsikos, D.; Kohrangi, M.; Bazzurro, P. Harmonizing Seismic Performance via Risk Targeted Spectra: State of the Art, Dependencies, and Implementation Proposals. *Earthq Eng Struct Dyn* **2023**, *52*, 4277–4299, doi:10.1002/eqe.3941.
15. Baltzopoulos, G.; Grella, A.; Iervolino, I. Some Issues in the Practical Application of Risk-Targeted Ground Motions. *Earthq Eng Struct Dyn* **2023**, doi:10.1002/eqe.4058.
16. Ricci, P.; Manfredi, V.; Noto, F.; Terrenzi, M.; Petrone, C.; Celano, F.; De Risi, M.T.; Camata, G.; Franchin, P.; Magliulo, G.; et al. Modeling and Seismic Response Analysis of Italian Code-Conforming Reinforced Concrete Buildings. *Journal of Earthquake Engineering* **2018**, *22*, 105–139, doi:10.1080/13632469.2018.1527733.
17. Vamvatsikos, D.; Allin Cornell, C. Incremental Dynamic Analysis. *Earthq Eng Struct Dyn* **2002**, *31*, 491–514, doi:10.1002/eqe.141.
18. Vamvatsikos, D.; Allin Cornell, C. Applied Incremental Dynamic Analysis. *Earthquake Spectra* **2004**, *20*, 523–553.
19. Cornell, C.A. Engineering Seismic Risk Analysis. *Bulletin of the Seismological Society of America* **1968**, *58*, 1583–1606.
20. Chioccarelli, E.; Cito, P.; Iervolino, I.; Giorgio, M. REASSESS V2.0: Software for Single- and Multi-Site Probabilistic Seismic Hazard Analysis. *Bulletin of Earthquake Engineering* **2019**, *17*, 1769–1793, doi:10.1007/s10518-018-00531-x.
21. Ambraseys, N.; Simpson, K.; Bommer, J. Prediction of Horizontal Response Spectra in Europe. *Earthq Eng Struct Dyn* **1996**, *25*, 371–400.
22. Meletti, C. et al. A Seismic Source Zone Model for the Seismic Hazard Assessment of the Italian Territory. *Tectonophysics* **2008**, *450*, 85–108.
23. Bojórquez, E.; Iervolino, I. Spectral Shape Proxies and Nonlinear Structural Response. *Soil Dynamics and Earthquake Engineering* **2011**, *31*, 996–1008, doi:10.1016/j.soildyn.2011.03.006.
24. Eads, L.; Miranda, E.; Lignos, D.G. Average Spectral Acceleration as an Intensity Measure for Collapse Risk Assessment. *Earthq Eng Struct Dyn* **2015**, 2057–2073, doi:10.1002/eqe.2575.
25. Kazantzi, A.K.; Vamvatsikos, D. Intensity Measure Selection for Vulnerability Studies for Building Classes. *Earthq Eng Struct Dyn* **2015**, *44*, 2677–2694, doi:10.1002/eqe.2603.
26. Baltzopoulos, G.; Baraschino, R.; Iervolino, I. On the Number of Records for Structural Risk Estimation in PBEE. *Earthq Eng Struct Dyn* **2019**, *48*, 489–506, doi:10.1002/eqe.3145.
27. Jayaram, N.; Baker, J.W. Statistical Tests of the Joint Distribution of Spectral Acceleration Values. *Bulletin of the Seismological Society of America* **2008**, *98*, 2231–2243, doi:10.1785/0120070208.
28. FEMA Quantification of Building Seismic Performance Factors. *Agency, Applied Technology Council for the Federal Emergency* **2009**, 421.
29. Suzuki, A.; Iervolino, I. Seismic Fragility of Code-Conforming Italian Buildings Based on SDoF Approximation. *Journal of Earthquake Engineering* **2021**, *25*, 2873–2907.
30. Baltzopoulos, G.; Grella, A.; Iervolino, I. Seismic Reliability Implied by Behavior-Factor-Based Design. *Earthq Eng Struct Dyn* **2021**, 1–21, doi:10.1002/eqe.3546.
31. Priestley, M.J.N. Performance Based Seismic Design. *Bulletin of the New Zealand Society for Earthquake Engineering* **2000**, *33*, 325–346.

32. Aschheim, M. Seismic Design Based on the Yield Displacement. *Earthquake Spectra* **2002**, *18*, 581–600.
33. Baltzopoulos, G.; Baraschino, R.; Iervolino, I.; Vamvatsikos, D. Dynamic Analysis of Single-Degree-of-Freedom Systems (DYANAS): A Graphical User Interface for OpenSees. *Eng Struct* **2018**, *177*, 395–408, doi:10.1016/j.engstruct.2018.09.078.
34. McKenna, F. OpenSees: A Framework for Earthquake Engineering Simulation. *Comput Sci Eng* **2011**, *13*, 58–66, doi:10.1109/MCSE.2011.66.
35. Baraschino, R.; Baltzopoulos, G.; Iervolino, I. R2R-EU: Software for Fragility Fitting and Evaluation of Estimation Uncertainty in Seismic Risk Analysis. *Soil Dynamics and Earthquake Engineering* **2020**, *132*, 106093, doi:10.1016/j.soildyn.2020.106093.
36. Iervolino, I. Assessing Uncertainty in Estimation of Seismic Response for PBEE. *Earthq Eng Struct Dyn* **2017**, *46*, 1711–1723, doi:10.1002/eqe.2883.
37. Luco, N.; Cornell, C.A. Structure-Specific Scalar Intensity Measures for near-Source and Ordinary Earthquake Ground Motions. *Earthquake Spectra* **2007**, *23*, 357–392, doi:10.1193/1.2723158.